

# Electronic structure of $ACo_2As_2$ ( $A = Ca, Sr, Ba, Eu$ ) studied using angle-resolved photoemission spectroscopy and theoretical calculations

R. S. Dhaka,<sup>1,2,\*</sup> Y. Lee,<sup>1</sup> V. K. Anand,<sup>1,†</sup> Abhishek Pandey,<sup>1,‡</sup>  
D. C. Johnston,<sup>1</sup> B. N. Harmon,<sup>1</sup> and Adam Kaminski<sup>1</sup>

<sup>1</sup>*The Ames Laboratory, U.S. DOE and Department of Physics and Astronomy, Iowa State University, Ames, Iowa 50011, USA*

<sup>2</sup>*Department of Physics, Indian Institute of Technology Delhi, Hauz Khas, New Delhi-110016, India*

(Dated: July 13, 2021)

We present a comprehensive study of the low-energy band structure and Fermi surface (FS) topology of  $ACo_2As_2$  ( $A = Ca, Sr, Ba, Eu$ ) using high-resolution angle-resolved photoemission spectroscopy. The experimental FS topology and band dispersion data are compared with theoretical full-potential linearized augmented-plane-wave (FP-LAPW) calculations, which yielded reasonably good agreement. We demonstrate that the FS maps of  $ACo_2As_2$  are significantly different from those of the parent compounds of Fe-based high-temperature superconductors. Further, the FSs of  $CaCo_2As_2$  do not show significant changes across its antiferromagnetic transition temperature. The band dispersions extracted in different momentum ( $k_x, k_y$ ) directions show a small electron pocket at the center and a large electron pocket at the corner of the Brillouin zone (BZ). The absence of the hole FS in these compounds does not allow nesting between pockets at the Fermi energy ( $E_F$ ), which is in contrast to  $AFe_2As_2$ -type parent compounds of the iron-based superconductors. Interestingly, we find that the hole bands are moved 300–400 meV below  $E_F$  depending on the  $A$  element. Moreover, the existence of nearly flat bands in the vicinity of  $E_F$  are consistent with the large density of states at  $E_F$ . These results are important to understand the physical properties as well as the possibility of the emergence of superconductivity in related materials.

## I. INTRODUCTION

Understanding the origin of the unconventional pairing mechanism in high-temperature superconductors, cuprates [1–3] and iron pnictides [4–12], is one of the most challenging issues in condensed-matter physics. In particular, the superconductivity (SC) in the iron pnictides has received enormous attention to find its intimate connection with the magnetic ordering [13, 14]. For example, the parent compound  $BaFe_2As_2$  shows a phase change from high temperature tetragonal to low temperature orthorhombic structure at  $\approx 135$  K along with an associated antiferromagnetic (AFM) spin density wave (SDW) transition. It is well known that the common method to induce high- $T_c$  superconductivity in these materials is to suppress the SDW ground state by different ways such as partial chemical substitution and/or application of external pressure [5–11, 13, 14]. One of the most intriguing aspects is to study how the long-range magnetic order and superconductivity are related in these materials [10, 15]. In this context, investigation of the electronic structure and Fermi surface (FS) topology using angle-resolved photoemission spectroscopy (ARPES) is vital [16–23]. The FS of  $BaFe_2As_2$  consists of a hole (at the  $\Gamma$  point) and an electron (at the  $X$  point) pockets, and their similar volumes suggest that the material

is compensated since the number of electrons and holes are equal. The nesting between the hole and the electron FSs can give SDW ordering [24–26] and play a pivotal role in driving the antiferromagnetic-paramagnetic phase transition [10, 25, 27]. The FSs of these materials show a remarkable reconstruction at low temperature due to the presence of an AFM SDW phase [16–21], and the suppression of magnetic ordering is linked to the onset of the SC dome [22, 23]. Interestingly, when Fe is replaced by Co in  $BaFe_2As_2$ , a rigid-band-like change in the band structure occurs and Lifshitz transitions are observed both at the onset and offset of the SC dome [23, 28–32]. On the other hand, no significant changes in the FS and band structure were observed for isoelectronic Ru substituted  $BaFe_2As_2$  across the SC dome [22, 33].

Therefore, one approach is to completely substitute Co/Ru at the Fe site and investigate how the band structure and FS topology are related to the magnetic ordering as well as the SC in these materials. In this direction, very interesting structural and magnetic properties of  $ACo_2As_2$  ( $A = Ca, Sr, Ba, Eu$ ) compounds have been reported [34–44]. For example, powder x-ray diffraction and magnetization measurements on  $CaCo_2As_2$  demonstrate the structure to be collapsed-tetragonal and A-type collinear AFM order is observed below  $T_N = 52$  K, respectively [35]. However, the resistivity and specific heat measurements show no evidence of the magnetic transition in  $CaCo_2As_2$  [35]. On the other hand,  $BaCo_2As_2$  exhibits paramagnetic behavior and no magnetic ordering is reported down to 1.8 K [44, 45]. Interestingly, these materials crystallize in the  $ThCr_2Si_2$ -type tetragonal structure and the  $c/a$  ratio of  $SrCo_2As_2$  is found to be 2.99, which is intermediate to those of normal-tetragonal  $BaCo_2As_2$  ( $c/a = 3.20$ ) exhibit-

\* Corresponding author: rsdhaka@physics.iitd.ac.in

† Present address: Department of Physics, University of Petroleum and Energy Studies, Dehradun, Uttarakhand, 248007, India

‡ Present address: Materials Physics Research Institute, School of Physics, University of the Witwatersrand, Johannesburg, Gauteng 2050, South Africa

ing ferromagnetic correlations and collapsed-tetragonal-antiferromagnetic  $\text{CaCo}_2\text{As}_2$  ( $c/a = 2.58$ ) [34]. Furthermore, the magnetization, NMR, and neutron diffraction measurements of  $\text{SrCo}_2\text{As}_2$  show no evidence for long-range magnetic ordering above 0.05 K [34, 36, 46, 47]. This is consistent with the isostructural  $\text{BaCo}_2\text{As}_2$  [44], but is in contrast to the AFM behavior of  $\text{CaCo}_2\text{As}_2$  [35, 41, 42]. More interestingly,  $\text{SrCo}_2\text{As}_2$  shows a negative (positive) thermal expansion coefficient along the  $c$  ( $a$ )-axis in the temperature range from  $\approx 7$  K to 300 K [34]. Also, the structural properties of  $\text{EuCo}_2\text{As}_2$  indicate a phase transition from tetragonal at ambient pressure to collapsed-tetragonal at high pressure [43]. The magnetization measurements at ambient pressure indicate that the effective paramagnetic moment at high temperatures arises mainly from the Eu spins with an appearance of AFM ordering  $\leq 39$  K [48].

Notably, there have been many reports on the structural and magnetic properties of these  $\text{ACo}_2\text{As}_2$  compounds [34–44]; however, detailed ARPES studies are very few [49–51] and not reported for  $\text{EuCo}_2\text{As}_2$ . Therefore, further investigations of the band structure and FSs of  $\text{ACo}_2\text{As}_2$  and comparison with the  $\text{AFe}_2\text{As}_2$  parent compounds are desired to shed light on the pairing mechanism of Fe-based superconductors.

In this paper, we report a comprehensive ARPES study of  $\text{ACo}_2\text{As}_2$  ( $A = \text{Ca, Sr, Ba, Eu}$ ) and present the FSs as well as low-energy band structures, which are found to be very different from  $\text{BaFe}_2\text{As}_2$  at the Fermi level. The experimental FSs and band dispersion data are compared with full-potential linearized augmented-plane-wave (FP-LAPW) calculations, which are found to be in reasonably good agreement. The corresponding band dispersion data show a small electron pocket at the center and large electron pocket at the corner of the Brillouin zone (BZ). This reveals that no obvious FS nesting is present in these compounds, which is in contrast to the parent compounds of Fe-based high- $T_c$  superconductors. Moreover, we observe that the hole bands are moved 300–400 meV below the  $E_F$  compared to the hole bands crossing  $E_F$  in the  $\text{AFe}_2\text{As}_2$  compounds. Here in case of  $\text{ACo}_2\text{As}_2$ , the rigid-band-like shift in the band structure results in the appearance of a small electron pocket at the  $\Gamma$  point [49–51]. Moreover, we find that the bands in the vicinity of  $E_F$  are reasonably flat, which are responsible for high intensity peak in the density of states (DOS) at  $E_F$  and important to understand the physical properties of these  $\text{ACo}_2\text{As}_2$  materials. In addition, there are no notable changes in the FS topology of  $\text{CaCo}_2\text{As}_2$  measured at, below, and above the AFM transition temperature.

## II. EXPERIMENTAL DETAILS

High-quality single crystals of  $\text{ACo}_2\text{As}_2$  ( $A = \text{Ca, Sr, Eu}$ ) were grown with Sn-flux whereas  $\text{BaCo}_2\text{As}_2$  out of self flux and the details of bulk physical property measurements and x-ray analysis can be found in

Refs. [34, 35, 37, 45]. We used a Scienta R4000 electron analyzer to perform high-resolution ARPES measurements at beamline 7.0.1 of the Advanced Light Source (ALS), Berkeley, California. All samples were cleaved *in situ* in an ultrahigh vacuum chamber having  $\leq 4 \times 10^{-11}$  mbar pressure, yielding flat mirror-like surfaces in the  $ab$  plane. The ARPES data were collected with  $\sim 20$  meV and  $\sim 0.3^\circ$  energy and momentum resolutions, respectively. Several samples from different batches were measured to reproduce the results of the Fermi surfaces and band structure. We use a gold sample to determine the Fermi energy.

We calculate the Fermi surfaces and band dispersions of  $\text{ACo}_2\text{As}_2$  with the FP-LAPW method using the local density approximation [52]. We use  $R_{\text{MT}} \times k_{\text{max}} = 8$  or 9 to find the self-consistent charge density, where the smallest muffin tin (MT) radius is multiplied by the maximum  $k$  value in the plane wave expansion basis. Here, the MT radii of 2.1, 2.3, 2.5, 2.5, 2.1, and 2.1 a.u. were taken for Ca, Sr, Ba, Eu, Co, and As, respectively. Note that 828  $k$ -points were selected in the irreducible BZ to perform the calculations until we reached the total energy convergence criterion of 0.01 mRy/ primitive cell. Also, we relaxed the As atom  $z$ -axis position to find a minimum total energy, which gave  $z_{\text{As}} = 0.3622, 0.3515, 0.3441$ , and  $0.3611$  for  $A = \text{Ca, Sr, Ba, and Eu}$ , respectively. To compute the FSs, we divide the  $-2\pi/a \leq (k_x, k_y) \leq 2\pi/a$  ranges of  $k_x, k_y$  planes with different  $k_z$  values into  $200 \times 200$  meshes.

## III. RESULTS AND DISCUSSION

In order to understand how the low-energy band structure changes between different members of  $\text{ACo}_2\text{As}_2$  family, in Figs. 1(a–d) we present the photoemission intensity maps of  $\text{ACo}_2\text{As}_2$  ( $A = \text{Ca, Sr, Ba, Eu}$ ) at  $E_F$  measured at  $k_z \approx 2\pi/c$ . To plot the FS maps, we have integrated the intensity of the photoelectrons within  $\pm 10$  meV about  $E_F$ . Interestingly, we find that the shape of the FSs of  $\text{ACo}_2\text{As}_2$  is more complicated [49, 50] than those of the parent  $\text{AFe}_2\text{As}_2$  compounds of the 122-family [22]. In particular, the FS map of  $\text{CaCo}_2\text{As}_2$  [Fig. 1(a)] clearly exhibits small elliptical pockets centered around the corner ( $X$  point) of the BZ. Additionally, we also observe four small pockets around the center ( $\Gamma$  point) of the BZ. In the case of  $\text{SrCo}_2\text{As}_2$  [Fig. 1(b)], the FS topology is slightly different in the sense that the elliptical pockets at the  $X$  point become straight and the four small pockets around the  $\Gamma$  point are now less visible. The FS of  $\text{BaCo}_2\text{As}_2$  in Fig. 1(c) is significantly different where the pockets at  $X$  point break into small segments, and the four small pockets around the  $\Gamma$  point are become smaller in size and change in shape. More interestingly, we observe a small circular pocket at the  $\Gamma$  point in the FS map of  $\text{EuCo}_2\text{As}_2$ . At the corner ( $X$  point) of the BZ, long straight segments of intensity pocket for the  $A = \text{Sr, Ba, and Eu}$  samples are clearly different in shape as com-

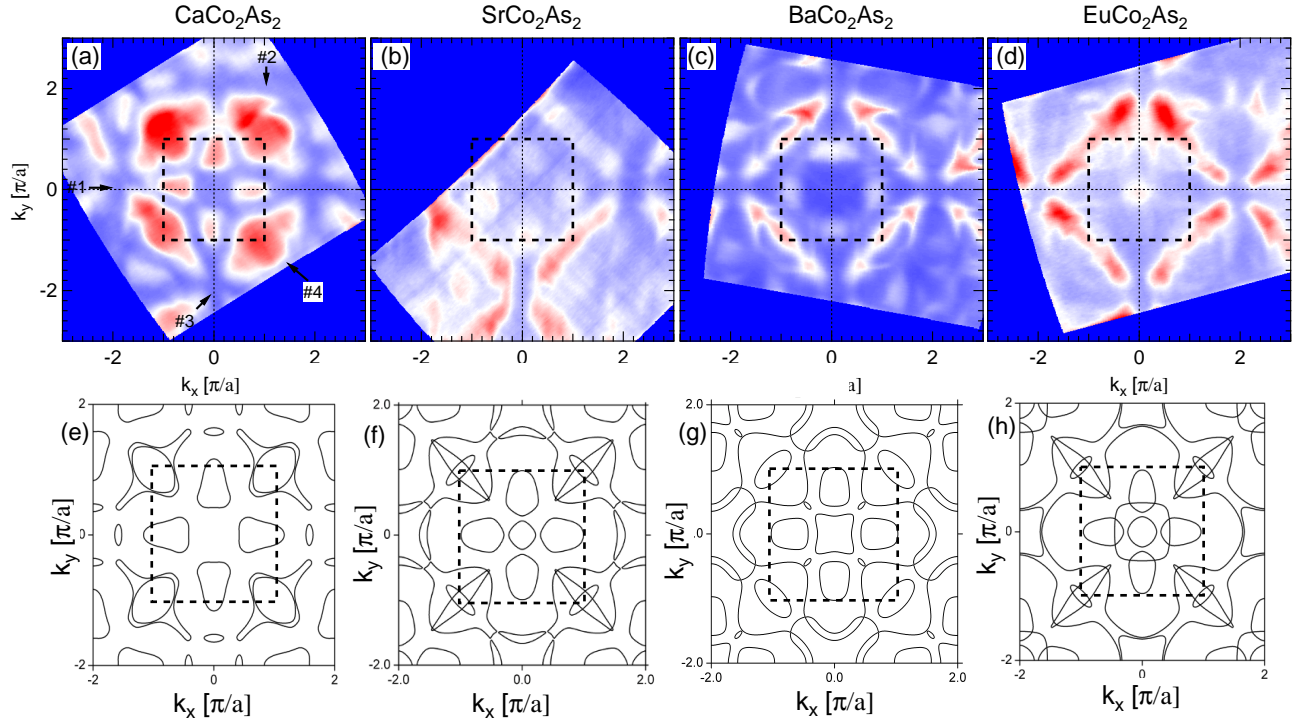


FIG. 1. Fermi surface maps of  $ACo_2As_2$  ( $A = Ca, Sr, Ba, Eu$ ) plotted by integrating the photoelectron intensity within  $\pm 10$  meV about  $E_F$ , for (a)  $CaCo_2As_2$  ( $T_S \approx 20$  K,  $h\nu = 135$  eV), (b)  $SrCo_2As_2$  ( $T_S \approx 90$  K,  $h\nu = 140$  eV), (c)  $BaCo_2As_2$  ( $T_S \approx 200$  K,  $h\nu = 135$  eV), and (d)  $EuCo_2As_2$  ( $T_S \approx 200$  K,  $h\nu = 135$  eV). The outline of the first Brillouin zone is shown by a black dashed square. The panels (e–h) are same as (a–d), but calculated. The panels (b, c, f, g) are reconstructed from our earlier publications [34, 49] for comparison within the  $ACo_2As_2$  family.

pared to  $CaCo_2As_2$ . In the case of  $A = Eu$ , the intensity of the four small electron pockets (along the  $k_x, k_y$  directions) around the center of the BZ almost disappeared as compared to  $CaCo_2As_2$ , see Figs. 1(a, d).

Interestingly, we observe a significant change in the FS topology of  $ACo_2As_2$  family by changing the element at  $A$  site (for example in the present study  $A = Ca, Sr, Ba$ , and  $Eu$ ) [34, 49, 50], as compared to the other related parent compounds  $AFe_2As_2$  [22, 53]. Moreover, the appearance of a small intensity pocket at the  $\Gamma(0,0)$  point at  $E_F$  in  $EuCo_2As_2$  [see Fig. 1(d)] clearly suggests a shift in the Fermi level, which may be different from the other  $ACo_2As_2$  ( $A = Ca, Sr, Ba$ ) compounds.

Therefore, to further understand the electronic structure of these samples, we performed theoretical calculations for all the samples at the same  $k_z$  points and compared the calculated FS maps in Figs. 1(e–h), respectively. In case of  $CaCo_2As_2$ , four patches of intensity (along the  $k_x, k_y$  directions) around the  $\Gamma$  point and large elliptical pockets across the  $X$  points are clearly seen in Fig. 1(e). Overall, the theoretically-calculated FS topology clearly shows significant changes between the  $Ca, Sr, Ba$ , and  $Eu$  members, see Figs. 1(e–h). Also, the FS maps of  $ACo_2As_2$  ( $A = Ca, Sr, Ba, Eu$ ) are very different from the other related parent compounds of the 122 family such as  $CaFe_2As_2$  and  $BaFe_2As_2$  [21, 53]. However, if we see the FS plotted about 400 meV below  $E_F$  (discussed

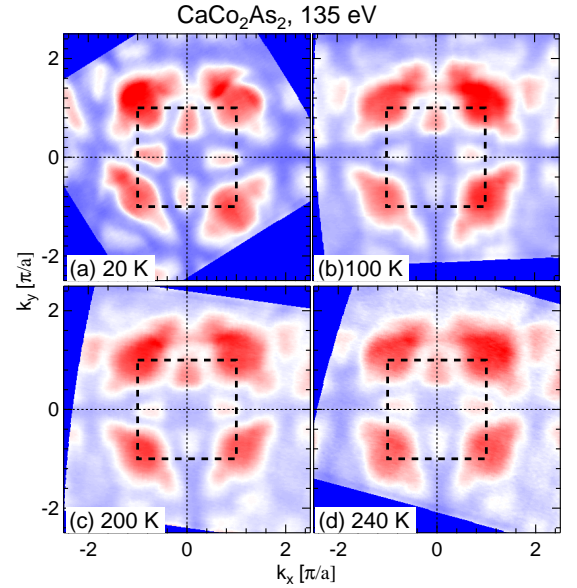


FIG. 2. Fermi surface maps of  $CaCo_2As_2$  measured with 135 eV photon energy and at different sample temperatures.

later) [49], it is very similar to that of  $BaFe_2As_2$ , where the FSs are roughly circular in shape and are roughly

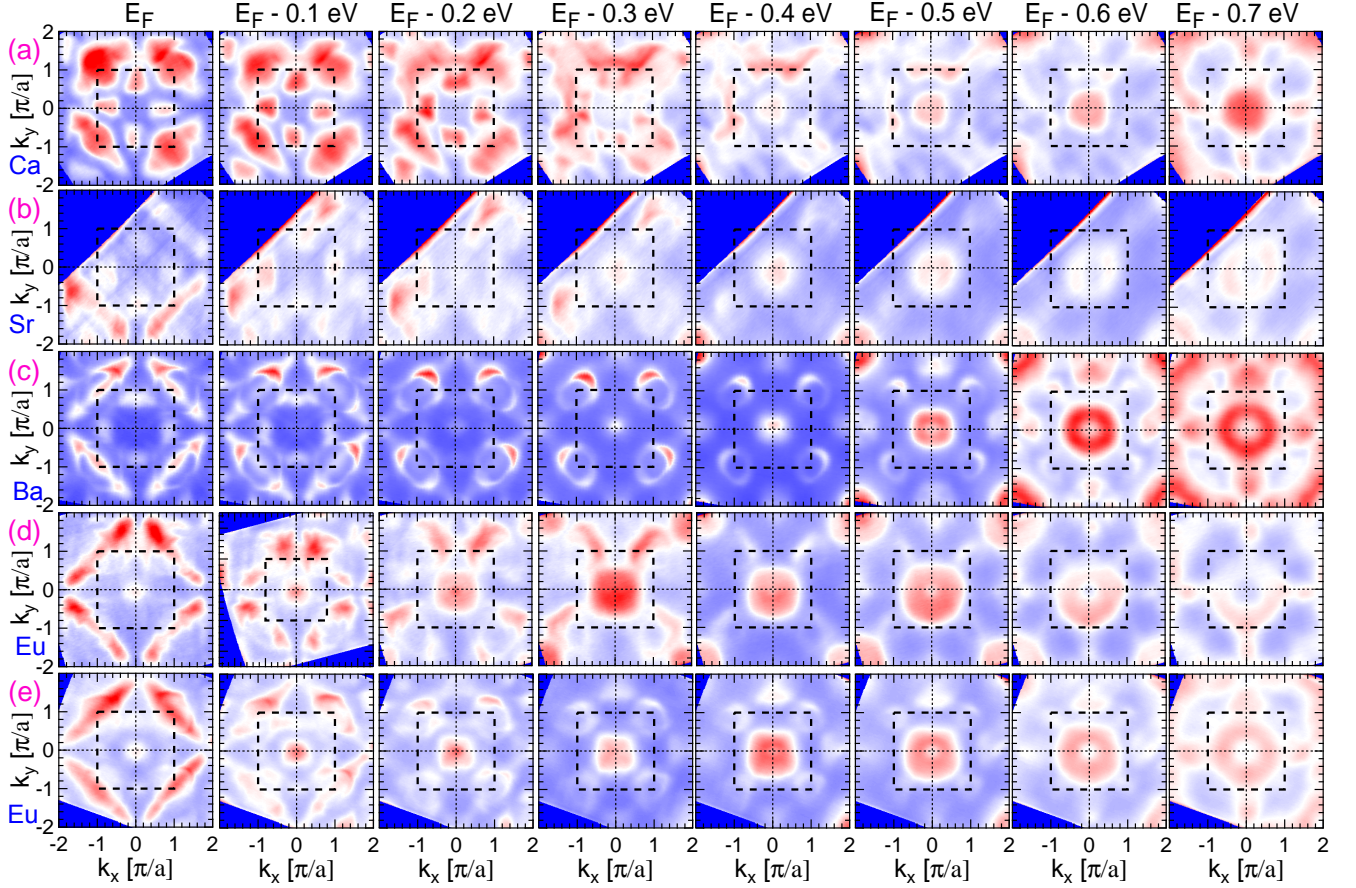


FIG. 3. The photoemission intensity maps of  $ACo_2As_2$  ( $A = Ca, Sr, Ba, Eu$ ) plotted at different binding energies, as marked on the top of each panel. Panel (a)  $CaCo_2As_2$  (135 eV, 20 K), panel (b) for  $SrCo_2As_2$  (140 eV, 90 K), panel (c) for  $BaCo_2As_2$  (135 eV, 200 K), and panels (d, e) for  $EuCo_2As_2$  [(d) 135 eV and (e) 115 eV, 200 K]. The intensity of the photoelectrons is integrated within  $\pm 10$  meV about the corresponding binding energy value in each panel.

similar in size [21]. This clearly indicates a shift of about 400 meV in the Fermi energy by completely replacing Fe with Co in these systems [49, 50]. It is important to note here that the overall shape of the measured FSs in Figs. 1(a–d) is in relatively good agreement with the respective calculations in Figs. 1(e–h).

As discussed above, in case of  $CaCo_2As_2$  sample, the magnetization measurements show an AFM transition at 52 K [35]. Also, it is important to note here that the ARPES studies of  $Ba(Fe_{1-x}Ru_x)_2As_2$  and  $Ba(Fe_{1-x}Co_x)_2As_2$  show significant changes in the band structure with sample temperature [27, 54]. Moreover, it was shown that temperature-dependent FS nesting may play an important role in driving the AFM-paramagnetic phase transition in these materials [20–23]. Therefore, to get more insights for understanding whether there are changes in the band structure of  $CaCo_2As_2$  with temperature across the AFM transition temperature ( $T_N$ ), we measured the FSs with 135 eV photon energy using a synchrotron radiation source. In Fig. 2, the FSs are shown at different sample temperatures from 20 to

240 K, which confirm that there are no notable differences in the FS topology measured below [Fig. 2(a)] and above [Figs. 2(b–d)] ( $T_N$ ). Further, as the FS of  $AFe_2As_2$  below  $T_N$  shows a reconstruction [23], which is clearly absent in the FS of  $CaCo_2As_2$  measured at 20 K, see Fig. 2(a). These results indicate that the electron correlations are moderate in the  $ACo_2As_2$  family, as the overall mass enhancement of the Co 3d electrons is found to be smaller [55] as compared to the Fe 3d electrons in  $AFe_2As_2$  based compounds [20–23].

In order to compare the FS topology at different binding energies, we show the  $(k_x, k_y)$  plots from 0 to 700 meV below  $E_F$  for all the samples in Fig. 3. For the  $CaCo_2As_2$ , we observe a decrease in the intensity of the small pockets around the zone center along with a shape change at the corner of the BZ, see panel (a) in Fig. 3. At 400 meV below  $E_F$ , a small pocket is clearly seen at the center of the BZ, which grows in size with further increase in the binding energy. At the same time, the shape of the pocket at the corner is very similar to that of the electron pocket observed in  $AFe_2As_2$  samples. Similar changes



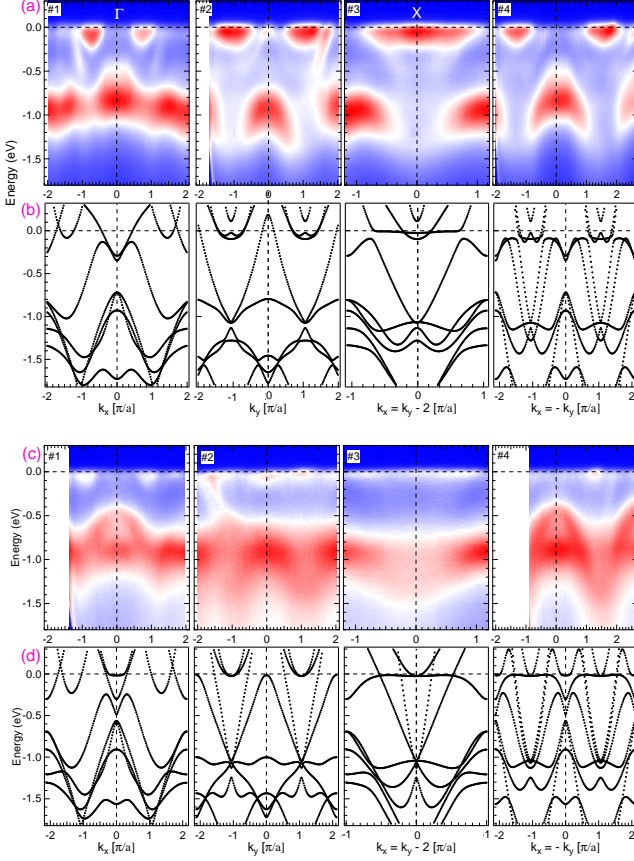


FIG. 4. Experimental band dispersion data of  $\text{CaCo}_2\text{As}_2$  (panel a) and  $\text{SrCo}_2\text{As}_2$  (panel c) measured with 135 eV and 140 eV photon energies, and the corresponding theoretical band dispersions in panels (b) and (d), respectively. The locations of the cuts #1, #2, #3 and #4 are marked in Fig. 1(a). In panels (c) and (d), cuts #1 and #3 are similar to the reported in our publication [34], reconstructed for comparison.

are observed for the  $\text{SrCo}_2\text{As}_2$  sample, as shown in panel (b) except that the center pocket appeared at around 300 meV below  $E_F$ , and the size of both the pockets at the center and at the corner of the BZ is almost similar at 400 meV. For the  $\text{BaCo}_2\text{As}_2$  sample, a small intensity of the central pocket is visible at 200 meV, see panel (c), and again the size of both pockets is similar at 300-400 meV below  $E_F$ . Interestingly, in case of the  $\text{EuCo}_2\text{As}_2$ , the central pocket is already visible at  $E_F$ , see panels (d, e), measured at 135 eV and 115 eV photon energies, respectively. Further, the size and shape of both pockets at the center and corner of the BZ look similar for all the samples at around 400 meV below  $E_F$  except for  $\text{EuCo}_2\text{As}_2$ . More carefully, if we compare the size of the pocket at the BZ center at 700 meV below  $E_F$  for all the samples, it qualitatively increases from Ca to Sr to Ba to Eu. These  $(k_x, k_y)$  plots of  $\text{ACo}_2\text{As}_2$  further motivated us to investigate the low-energy band structure in detail by plotting the band dispersion and comparing them with those calculated theoretically along different momentum  $(k_x, k_y)$

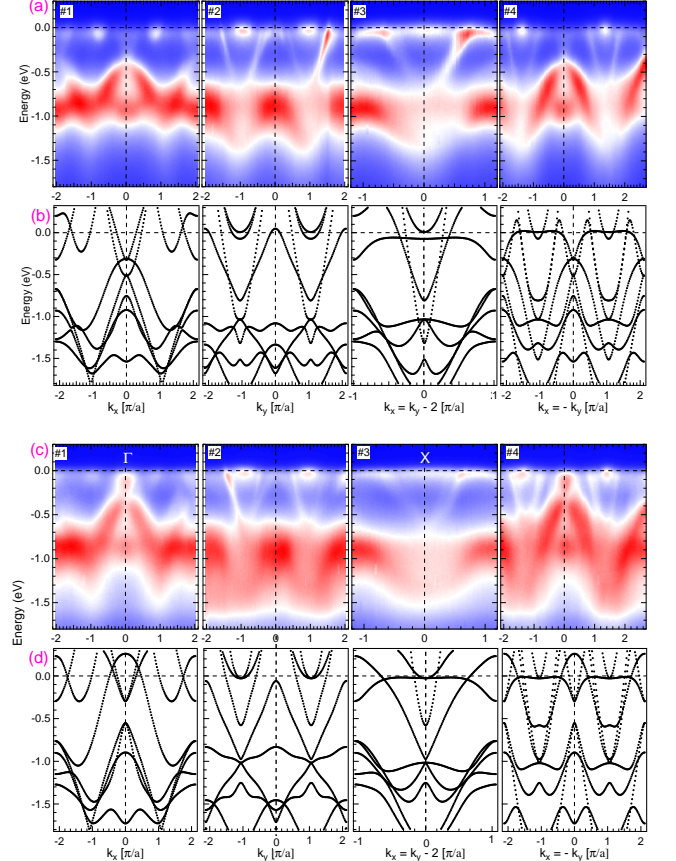


FIG. 5. Experimental band dispersion data of  $\text{BaCo}_2\text{As}_2$  (panel a) and  $\text{EuCo}_2\text{As}_2$  (panel c) measured with 135 eV photon energy. The plots in panels (b) and (d) are the corresponding theoretical band dispersions. The locations of the cuts #1, #2, #3 and #4 are marked in Fig. 1(a).

directions.

Therefore, to elucidate the character of these FS pockets, we extracted in-plane dispersions for all the samples and shown the energy-momentum intensity plots in Figs. 4 and 5 along the four different cuts in Figs. 4 and 5 along the four different cuts #1, #2, #3 and #4. These cuts are from  $(k_x, k_y) = (-2\pi, 0 \text{ to } 2\pi, 0)$ ,  $(2\pi, \pi \text{ to } -2\pi, -\pi)$ ,  $(0, -2\pi \text{ to } 2\pi, 0)$ ,  $(-2\pi, 2\pi \text{ to } 2\pi, -2\pi)$ , respectively, as marked in Fig. 1(a). The band dispersions measured with 135 eV photon energy are shown in Fig. 4 for the  $\text{ACo}_2\text{As}_2$  ( $A = \text{Ca, Sr}$ ) samples. The photoelectron intensity along the cut #1 at the center of the BZ ( $\Gamma$  point) is not very clear for these samples; however, we clearly observe two small electron pockets centered at the Fermi momenta of  $k_{Fx} \approx \pm 0.7\pi/a$ . Interestingly, the top of the hole pocket at the center of the BZ is clearly seen at about 400 meV below  $E_F$ . Moreover, we find a large electron pocket with  $k_{Fy} = \pm 0.65\pi/a$  in the band dispersion plotted along the cut #2 at the corner of the first BZ at  $X = (\pi, \pi)$ . In the cut #3, the data show a large electron pocket with  $k_F = \pm 0.65\pi/a$  and high intensity peak at the  $X$  point. For comparison, we have also plotted the data along the cut #4, which again

shows large electron pockets at the  $X$  points. To get more insights, it is important to compare the experimental results with theoretical calculations, and therefore, we present the calculated band dispersions in the lower panels for Fig. 4 along all four different cuts. We find a reasonable qualitative agreement between the theoretical and measured data.

Moreover, in Fig. 5, we show the low-energy band structure of  $\text{BaCo}_2\text{As}_2$  and  $\text{EuCo}_2\text{As}_2$  samples to understand the character of the FS pockets. We note here that the band dispersions of  $\text{BaCo}_2\text{As}_2$  are very similar to those of  $\text{SrCo}_2\text{As}_2$  except that the small-intensity electron-like bands are visible at the center of the BZ for  $\text{BaCo}_2\text{As}_2$ , which are found to be slightly stronger when measured with  $h\nu = 85$  eV in Ref. [49]. Also, the slope of the hole bands is more slanting in  $\text{ACo}_2\text{As}_2$  ( $A = \text{Sr}, \text{Ba}$ ) in comparison to  $\text{CaCo}_2\text{As}_2$ , see for example cuts #1 and #4 in Figs. 4 and 5.

It is intriguing to see the band structure of  $\text{EuCo}_2\text{As}_2$ , which is found to be significantly different from the other  $\text{ACo}_2\text{As}_2$  ( $A = \text{Ca}, \text{Sr}, \text{Ba}$ ) samples, see Figs. 4 and 5. We observe that the intensity of two smaller electron pockets at Fermi momenta  $k_{Fx} = \pm 0.9\pi/a$  reduced significantly and the top of the hole band at the center of the BZ ( $\Gamma$  point) is about 300 meV below  $E_F$ , see along the cut #1. This indicates that in the case of  $\text{EuCo}_2\text{As}_2$ , the rigid band shift at the center of the BZ is smaller ( $\approx 300$  meV) than in the other  $\text{ACo}_2\text{As}_2$  ( $A = \text{Ca}, \text{Sr}, \text{Ba}$ ) compounds (400 meV). Therefore, the Fermi momentum of the electron pocket at the  $\Gamma$  point  $k_{Fx} = \pm 0.15\pi/a$  is also slightly smaller than in  $\text{BaCo}_2\text{As}_2$  [49]. At the corner of the first BZ [ $X = (\pi, \pi)$ ], we observe a larger electron pocket for  $\text{ACo}_2\text{As}_2$  with  $k_F = \pm 0.65\pi/a$  (along both the cuts #2 and #3) as compared to the  $\text{AFe}_2\text{As}_2$  compounds [22]. The data through cut #4 again confirm the presence of large electron pockets at the  $X$  points and a smaller electron pocket at the  $\Gamma$  point. The band structure plots obtained from the FP-LAPW calculations, shown in the lower panels of Fig. 5, are in reasonable agreement with the experimentally-observed band dispersions.

Now we discuss the broad comparison of the band structure and FS topology between  $\text{ACo}_2\text{As}_2$  and  $\text{AFe}_2\text{As}_2$  compounds. Overall, the electronic DOS( $E$ ) of the  $\text{ACo}_2\text{As}_2$  samples are found to be similar to those of the Fe-based compounds. However, we observe a band shift of 300–500 meV below  $E_F$  due to extra  $d$  electron in Co as compared to Fe [34, 44, 49, 56], which may reflect the high intensity peak at  $E_F$ . Note that the Co  $d_{x^2-y^2}$  orbital has a larger bandwidth (between  $-5$  eV and  $2$  eV) than the Fe  $d$  orbitals (from  $-2$  eV to  $2$  eV) [24]. Therefore, a complex multi-band Fermi surface is observed in the ARPES measurements on the  $\text{ACo}_2\text{As}_2$  compounds along with the large DOS at  $E_F$  with no apparent nesting [49, 50]. In this scenario, the band structure of  $\text{ACo}_2\text{As}_2$  [55] appears significantly different at  $E_F$  with respect to that of  $\text{BaFe}_2\text{As}_2$ . Also, as noted above,  $\text{CaCo}_2\text{As}_2$  shows magnetic ordering at low temperature; however, APRES measurements across the magnetic transition indicate no

significant changes in the band structure. Similarly, a complex FS structure of  $\text{EuRh}_2\text{As}_2$  and  $\text{BaNi}_2\text{As}_2$  has been reported using ARPES, but no signature of band folding due to magnetic ordering was observed, which indicates a weak coupling between layers [57, 58]. Moreover, a significant decrease in electronic correlation is reported in  $\text{BaCr}_2\text{As}_2$  [59, 60]. Note that in the  $\text{ACo}_2\text{As}_2$  compounds a considerable decrease in interlayer distance and  $z_{\text{As}}$  results in different correlation strengths [55] when compared with iron pnictides [61].

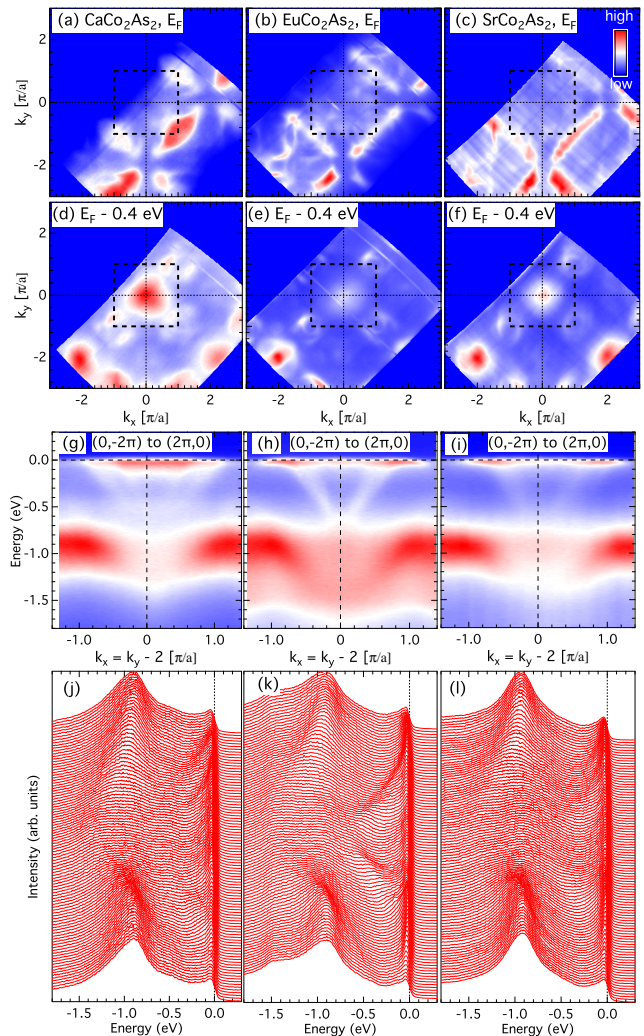


FIG. 6. (a–c) Fermi surface (FS) maps of  $\text{ACo}_2\text{As}_2$  ( $A = \text{Ca}, \text{Eu}, \text{Sr}$ ) measured with photon energy of 100 eV and at 90 K, where the first BZ boundaries are shown by black-dashed square. (d–f) Photoemission intensity maps are plotted at  $E_F - 0.4$  eV. These maps in (a–f) are constructed by integrating the intensity of the photoelectrons within  $\pm 10$  meV. (g–i) The band dispersions along the  $(0, -2\pi)$  to  $(2\pi, 0)$  direction from (a–c), respectively, and the corresponding energy dispersive curves (EDCs) are shown in (j–l).

Finally, we compare the FSs and low-energy band structures, in Fig. 6 of  $\text{ACo}_2\text{As}_2$  ( $A = \text{Ca}, \text{Eu}, \text{Sr}$ ) mea-

sured at 90 K with 100 eV photon energy. The intensity of photoelectrons along  $(k_x, k_y)$  is plotted at  $E_F$  in Figs. 6(a-c) and at 400 meV below  $E_F$  in Figs. 6(d-f). The FS plots at  $E_F$  show a long segment of intensity across the  $X$  points (corners of the BZ). The FS plots at 400 meV below  $E_F$  show clear changes in the FS shape at the  $X$  point, which changes from a large segment to an oval-shape pocket and approximately similar size as the pocket at the center of the BZ ( $\Gamma$  point). These results demonstrate the rigid band-like shift of 300-400 meV (depending on  $A$ ) below  $E_F$  for  $ACo_2As_2$  as compared to  $AFe_2As_2$ . Figures 6(g-i) show the band dispersion data plotted across the corner of the BZ ( $X$  point) i.e. from  $(0, -2\pi)$  to  $(2\pi, 0)$  and the corresponding energy dispersive curves (EDCs) are shown in Figs. 6(j-l). Again, for all these compounds we observe a large electron pocket at the  $X$  point and the bottom of this pocket is about 500 meV below  $E_F$ . More interestingly, we reveal a rather large flat band, driven by the Co  $3d_{x^2-y^2}$  orbital, in close vicinity of  $E_F$  with strong intensity near the  $X$  point in both the experimental and calculated data of  $ACo_2As_2$  compounds [49], as shown in Fig. 4 [cuts #2, #3 and #4 of panel (a)] as well as in Fig. 6. In ARPES measurements on the  $Fe_{1.03}Te_{0.94}S_{0.06}$  superconductor, Starowicz *et al.* observed a flat band at the Fermi level, which gives rise to high density of states at  $E_F$  [62]. This was explained in terms of as a Van Hove singularity, which is believed to play an important role in the emergence of superconductivity in Fe-based compounds [62]. The presence of a large density of states near  $E_F$  due to a nearly flat band at the corner of the BZ is crucial to understand the physical properties of the  $ACo_2As_2$  compounds.

#### IV. CONCLUSIONS

We have presented a comprehensive study of the electronic properties of the  $ACo_2As_2$  ( $A = Ca, Sr,$

$Ba$ , and  $Eu$ ) compounds using ARPES and theoretical FP-LAPW calculations. The FSs of these compounds are different from those of the parent compounds of FeAs-based high-temperature superconductors. The band dispersion data show a small electron pocket at the center and large electron pockets at the corner of the Brillouin zone. The experimental data agree reasonably well with the theoretical calculations. The absence of the FS nesting in  $ACo_2As_2$  is in contrast to the  $AFe_2As_2$  compounds. However, the top of the hole bands is found to be moved 300–400 meV below  $E_F$  (depending on  $A$ ) resulting an appearance of a small electron pocket at the center of the BZ. More interestingly, we observe large flat bands near  $E_F$ , which result in a large density of states and could be responsible for the interesting physical properties of these materials. Furthermore, no significant changes are observed in the FS topology of  $CaCo_2As_2$  between 20 and 300 K across the AFM transition. We discuss similarities and differences in the electronic properties of  $ACo_2As_2$  with respect to the parent  $AFe_2As_2$  compounds of 122 family.

#### V. ACKNOWLEDGMENTS

We thank Aaron Bostwick and Eli Rotenberg for excellent support at the ALS. This research was supported by the U.S. Department of Energy, Office of Basic Energy Sciences, Division of Materials Sciences and Engineering. Ames Laboratory is operated for the U.S. Department of Energy by Iowa State University under Contract No. DE-AC02-07CH11358. The Advanced Light Source is supported by the Office of Basic Energy Sciences, U. S. Department of Energy under Contract No. DE-AC02-05CH11231. RSD also acknowledges the support by BRNS through a DAE Young Scientist Research Award with Project Sanction No. 34/20/12/2015/BRNS.

- 
- [1] J. G. Bednorz and K. A. Müller, Possible high- $T_c$  superconductivity in the Ba-La-Cu-O system, *Z. Phys. B* **64**, 189 (1986).
  - [2] A. Schilling, M. Cantoni, J. D. Guo, and H. R. Ott, Superconductivity above 130 K in the Hg-Ba-Ca-Cu-O system, *Nature* **363**, 56 (1993).
  - [3] C. W. Chu, L. Gao, Z. J. Huang, R. L. Meng, and Y. Y. Xue, Superconductivity above 150 K in  $HgBa_2Ca_2Cu_3O_{8+\delta}$  at high pressures, *Nature* **365**, 323 (1993).
  - [4] Y. Kamihara, T. Watanabe, M. Hirano, and H. Hosono, Iron-Based Layered Superconductor  $La(O_{1-x}F_x)FeAs$  ( $x = 0.05-0.12$ ) with  $T_c = 26$  K, *J. Am. Chem. Soc.* **130**, 3296 (2008).
  - [5] H. Takahashi, K. Igawa, K. Arii, Y. Kamihara, M. Hirano, and H. Hosono, Superconductivity at 43 K in an iron-based layered compound  $LaO_{1-x}F_xFeAs$ , *Nature* **453**, 376 (2008).
  - [6] X. H. Chen, T. Wu, G. Wu, R. H. Liu, H. Chen, and D. F. Fang, Superconductivity at 43 K in  $SmFeAsO_{1-x}F_x$ , *Nature* **453**, 761 (2008).
  - [7] G. F. Chen, Z. Li, D. Wu, G. Li, W. Z. Hu, J. Dong, P. Zheng, J. L. Luo, and N. L. Wang, Superconductivity at 41 K and its competition with spin-density-wave instability in layered  $CeO_{1-x}F_xFeAs$ , *Phys. Rev. Lett.* **100**, 247002 (2008).
  - [8] M. Rotter, M. Tegel, and D. Johrendt, Superconductivity at 38 K in the iron arsenide  $(Ba_{1-x}K_x)Fe_2As_2$ , *Phys. Rev. Lett.* **101**, 107006 (2008).
  - [9] H. Q. Yuan, J. Singleton, F. F. Balakirev, S. A. Baily, G. F. Chen, J. L. Luo, and N. L. Wang, Nearly isotropic superconductivity in  $(Ba, K)Fe_2As_2$ , *Nature* **457**, 565 (2009).
  - [10] C. de la Cruz, Q. Huang, J. W. Lynn, L. Jiying, W. Ratcliff II, J. L. Zarestki, H. A. Mook, G. F. Chen, J. L. Luo, N. L. Wang, and P. Dai, Magnetic order close to su-

- perconductivity in the iron-based layered  $\text{LaO}_{1-x}\text{F}_x\text{FeAs}$  systems, *Nature* **453**, 899 (2008).
- [11] A. S. Sefat, R. Jin, M. A. McGuire, B. C. Sales, D. J. Singh, and D. Mandrus, Superconductivity at 22 K in Co-doped  $\text{BaFe}_2\text{As}_2$  crystals, *Phys. Rev. Lett.* **101**, 117004 (2008).
  - [12] F. Wang and D.-H. Lee, The electron-pairing mechanism of iron-based superconductors, *Science* **332**, 200 (2011).
  - [13] D. C. Johnston, The puzzle of high temperature superconductivity in layered iron pnictides and chalcogenides, *Adv. Phys.* **59**, 803 (2010).
  - [14] P. C. Canfield and S. L. Bud'ko, FeAs-based superconductivity: a case study of the effects of transition metal doping on  $\text{BaFe}_2\text{As}_2$ , *Annu. Rev. Condens. Matter Phys.* **1**, 27 (2010).
  - [15] D. K. Pratt, W. Tian, A. Kreyssig, J. L. Zarestky, S. Nandi, N. Ni, S. L. Bud'ko, P. C. Canfield, A. I. Goldman, and R. J. McQueeney, Coexistence of competing antiferromagnetic and superconducting phases in the underdoped  $\text{Ba}(\text{Fe}_{0.953}\text{Co}_{0.047})_2\text{As}_2$  compound using x-ray and neutron scattering techniques, *Phys. Rev. Lett.* **103**, 087001 (2009).
  - [16] G. Liu, H. Liu, L. Zhao, W. Zhang, X. Jia, J. Meng, X. Dong, J. Zhang, G. F. Chen, G. Wang, Y. Zhou, Y. Zhu, X. Wang, Z. Xu, C. Chen, and X. J. Zhou, Band-structure reorganization across the magnetic transition in  $\text{BaFe}_2\text{As}_2$  seen via high-resolution angle-resolved photoemission, *Phys. Rev. B* **80**, 134519 (2009).
  - [17] L. X. Yang, Y. Zhang, H. W. Ou, J. F. Zhao, D. W. Shen, B. Zhou, J. Wei, F. Chen, M. Xu, C. He, Y. Chen, Z. D. Wang, X. F. Wang, T. Wu, G. Wu, X. H. Chen, M. Arita, K. Shimada, M. Taniguchi, Z. Y. Lu, T. Xiang, and D. L. Feng, Electronic structure and unusual exchange splitting in the spin-density-wave state of the  $\text{BaFe}_2\text{As}_2$  parent compound of iron-based superconductors, *Phys. Rev. Lett.* **102**, 107002 (2009).
  - [18] Y. Zhang, J. Wei, H. W. Ou, J. F. Zhao, B. Zhou, F. Chen, M. Xu, C. He, G. Wu, H. Chen, M. Arita, K. Shimada, H. Namatame, M. Taniguchi, X. H. Chen, and D. L. Feng, Unusual doping dependence of the electronic structure and coexistence of spin-density-wave and superconductor phases in single crystalline  $\text{Sr}_{1-x}\text{K}_x\text{Fe}_2\text{As}_2$ , *Phys. Rev. Lett.* **102**, 127003 (2009).
  - [19] M. Yi, D. H. Lu, J. G. Analytis, J.-H. Chu, S.-K. Mo, R.-H. He, M. Hashimoto, R. G. Moore, I. I. Mazin, D. J. Singh, Z. Hussain, I. R. Fisher, and Z.-X. Shen, Unconventional electronic reconstruction in undoped  $(\text{Ba}, \text{Sr})\text{Fe}_2\text{As}_2$  across the spin density wave transition, *Phys. Rev. B* **80**, 174510 (2009).
  - [20] Chang Liu, T. Kondo, Ni Ni, A. D. Palczewski, A. Bostwick, G. D. Samolyuk, R. Khasanov, M. Shi, E. Rotenberg, S. L. Bud'ko, P. C. Canfield, and A. Kaminski, Three- to two-dimensional transition of the electronic structure in  $\text{CaFe}_2\text{As}_2$ : a parent compound for an iron arsenic high-temperature superconductor, *Phys. Rev. Lett.* **102**, 167004 (2009).
  - [21] T. Kondo, R. M. Fernandes, R. Khasanov, C. Liu, A. D. Palczewski, N. Ni, M. Shi, A. Bostwick, E. Rotenberg, J. Schmalian, S. L. Bud'ko, P. C. Canfield, and A. Kaminski, Unexpected Fermi-surface nesting in the pnictide parent compounds  $\text{BaFe}_2\text{As}_2$  and  $\text{CaFe}_2\text{As}_2$  revealed by angle-resolved photoemission spectroscopy, *Phys. Rev. B* **81**, 060507(R) (2010).
  - [22] R. S. Dhaka, C. Liu, R. M. Fernandes, R. Jiang, C. P. Strehlow, T. Kondo, A. Thaler, J. Schmalian, S. L. Bud'ko, P. C. Canfield, and A. Kaminski, What controls the phase diagram and superconductivity in Ru substituted  $\text{BaFe}_2\text{As}_2$ ?, *Phys. Rev. Lett.* **107**, 267002 (2011).
  - [23] C. Liu, T. Kondo, R. M. Fernandes, A. D. Palczewski, E. D. Mun, N. Ni, A. N. Thaler, A. Bostwick, E. Rotenberg, J. Schmalian, S. L. Bud'ko, P. C. Canfield, and A. Kaminski, Evidence for a Lifshitz transition in electron-doped iron arsenic superconductors at the onset of superconductivity, *Nature Phys.* **6**, 419 (2010).
  - [24] D. J. Singh and M.-H. Du, Density functional study of  $\text{LaFeAsO}_{1-x}\text{F}_x$ : a low carrier density superconductor near itinerant magnetism, *Phys. Rev. Lett.* **100**, 237003 (2008).
  - [25] I. I. Mazin, Superconductivity gets an iron boost, *Nature* **464**, 183 (2010).
  - [26] I. I. Mazin, D. J. Singh, M. D. Johannes, and M. H. Du, Unconventional superconductivity with a sign reversal in the order parameter of  $\text{LaFeAsO}_{1-x}\text{F}_x$ , *Phys. Rev. Lett.* **101**, 057003 (2008).
  - [27] R. S. Dhaka, S. E. Hahn, E. Razzoli, R. Jiang, M. Shi, B. N. Harmon, A. Thaler, S. L. Bud'ko, P. C. Canfield, and A. Kaminski, Unusual temperature dependence of band dispersion in  $\text{Ba}(\text{Fe}_{1-x}\text{Ru}_x)_2\text{As}_2$  and its consequences for antiferromagnetic ordering, *Phys. Rev. Lett.* **110**, 067002 (2013).
  - [28] C. Liu, A. D. Palczewski, R. S. Dhaka, T. Kondo, R. M. Fernandes, E. D. Mun, H. Hodovanets, A. N. Thaler, J. Schmalian, S. L. Bud'ko, P. C. Canfield, and A. Kaminski, Importance of the Fermi-surface topology to the superconducting state of the electron-doped pnictide  $\text{Ba}(\text{Fe}_{1-x}\text{Co}_x)_2\text{As}_2$ , *Phys. Rev. B* **84**, 020509(R) (2011).
  - [29] S. Thirupathaiah, S. de Jong, R. Ovsyannikov, H. A. Dürr, A. Varykhalov, R. Follath, Y. Huang, R. Huisman, M. S. Golden, Y.-Z. Zhang, H. O. Jeschke, R. Valentí, A. Erb, A. Gloskovskii, and J. Fink, Orbital character variation of the Fermi surface and doping dependent changes of the dimensionality in  $\text{BaFe}_{2-x}\text{Co}_x\text{As}_2$  from angle-resolved photoemission spectroscopy, *Phys. Rev. B* **81**, 104512 (2010).
  - [30] V. Brouet, M. Marsi, B. Mansart, A. Nicolaou, A. Taleb-Ibrahimi, P. Le Fèvre, F. Bertran, F. Rullier-Albenque, A. Forget, and D. Colson, Nesting between hole and electron pockets in  $\text{Ba}(\text{Fe}_{1-x}\text{Co}_x)_2\text{As}_2$  ( $x = 0-0.3$ ) observed with angle-resolved photoemission, *Phys. Rev. B* **80**, 165115 (2009).
  - [31] Y. Sekiba, T. Sato, K. Nakayama, K. Terashima, P. Richard, J. H. Bowen, H. Ding, Y. -M. Xu, L. J. Li, G. H. Cao, Z. -A. Xu and T. Takahashi, Electronic structure of heavily electron-doped  $\text{BaFe}_{1.7}\text{Co}_{0.3}\text{As}_2$  studied by angle-resolved photoemission, *New J. Phys.* **11**, 025020 (2009).
  - [32] S. Ideta, T. Yoshida, I. Nishi, A. Fujimori, Y. Kotani, K. Ono, Y. Nakashima, S. Yamaichi, T. Sasagawa, M. Nakajima, K. Kihou, Y. Tomioka, C. H. Lee, A. Iyo, H. Eisaki, T. Ito, S. Uchida, and R. Arita, Dependence of carrier doping on the impurity potential in transition-metal-substituted FeAs-based superconductors, *Phys. Rev. Lett.* **110**, 107007 (2013).
  - [33] L. Liu, T. Mikami, S. Ishida, K. Koshiishi, K. Okazaki, T. Yoshida, H. Suzuki, M. Horio, L. C. C. Ambolode II, J. Xu, H. Kumigashira, K. Ono, M. Nakajima, K. Kihou, C. H. Lee, A. Iyo, H. Eisaki, T. Kakeshita, S.



- Uchida, and A. Fujimori, In-plane electronic anisotropy in the antiferromagnetic orthorhombic phase of isovalent-substituted  $\text{Ba}(\text{Fe}_{1-x}\text{Ru}_x)_2\text{As}_2$ , *Phys. Rev. B* **92**, 094503 (2015).
- [34] A. Pandey, D. G. Quirinale, W. Jayasekara, A. Sapkota, M. G. Kim, R. S. Dhaka, Y. Lee, T. W. Heitmann, P. W. Stephens, V. Ogloblich, A. Kreyssig, R. J. McQueeney, A. I. Goldman, A. Kaminski, B. N. Harmon, Y. Furukawa, and D. C. Johnston, Crystallographic, electronic, thermal and magnetic properties of single-crystal  $\text{SrCo}_2\text{As}_2$ , *Phys. Rev. B* **88**, 014526 (2013).
- [35] V. K. Anand, R. S. Dhaka, Y. Lee, B. N. Harmon, A. Kaminski, and D. C. Johnston, Physical properties of metallic antiferromagnetic  $\text{CaCo}_{1.86}\text{As}_2$  single crystals, *Phys. Rev. B* **89**, 214409 (2014).
- [36] B. Li, B. G. Ueland, W. T. Jayasekara, D. L. Abernathy, N. S. Sangeetha, D. C. Johnston, Q. -P. Ding, Y. Furukawa, P. P. Orth, A. Kreyssig, A. I. Goldman, and R. J. McQueeney, Competing magnetic phases and itinerant magnetic frustration in  $\text{SrCo}_2\text{As}_2$ , *Phys. Rev. B* **100**, 054411 (2019).
- [37] N. S. Sangeetha, V. K. Anand, E. Cuervo-Reyes, V. Smetana, A.-V. Mudring, and D. C. Johnston, Enhanced moments of Eu in single crystals of the metallic helical antiferromagnet  $\text{EuCo}_{2-y}\text{As}_2$ , *Phys. Rev. B* **97**, 144403 (2018).
- [38] A. Sapkota, B. G. Ueland, V. K. Anand, N. S. Sangeetha, D. L. Abernathy, M. B. Stone, J. L. Niedziela, D. C. Johnston, A. Kreyssig, A. I. Goldman, and R. J. McQueeney, Effective one-dimensional coupling in the highly frustrated square-lattice itinerant magnet  $\text{CaCo}_{2-y}\text{As}_2$ , *Phys. Rev. Lett.* **119**, 147201 (2017).
- [39] Q.-P. Ding, N. Higa, N. S. Sangeetha, D. C. Johnston, and Y. Furukawa, NMR determination of an incommensurate helical antiferromagnetic structure in  $\text{EuCo}_2\text{As}_2$ , *Phys. Rev. B* **95**, 184404 (2017).
- [40] W. T. Jayasekara, U. S. Kaluarachchi, B. G. Ueland, A. Pandey, Y. B. Lee, V. Taufour, A. Sapkota, K. Kothapalli, N. S. Sangeetha, G. Fabbris, L. S. I. Veiga, Y. Feng, A. M. dos Santos, S. L. Bud'ko, B. N. Harmon, P. C. Canfield, D. C. Johnston, A. Kreyssig, and A. I. Goldman, Pressure-induced collapsed-tetragonal phase in  $\text{SrCo}_2\text{As}_2$ , *Phys. Rev. B* **92**, 224103 (2015).
- [41] J. J. Ying, Y. J. Yan, A. F. Wang, Z. J. Xiang, P. Cheng, G. J. Ye, and X. H. Chen, Metamagnetic transition in  $\text{Ca}_{1-x}\text{Sr}_x\text{Co}_2\text{As}_2$  ( $x = 0$  and  $0.1$ ) single crystals, *Phys. Rev. B* **85**, 214414 (2012).
- [42] B. Cheng, B. F. Hu, R. H. Yuan, T. Dong, A. F. Fang, Z. G. Chen, G. Xu, Y. G. Shi, P. Zheng, J. L. Luo, and N. L. Wang, Field-induced spin-flop transitions in single-crystalline  $\text{CaCo}_2\text{As}_2$ , *Phys. Rev. B* **85**, 144426 (2012).
- [43] M. Bishop, W. Uho, G. Tsoi, Y. K. Vohra, A. S. Sefat, and B. C. Sales, Formation of collapsed tetragonal phase in  $\text{EuCo}_2\text{As}_2$  under high pressure, *J. Phys.: Condens. Matter* **22**, 425701 (2010).
- [44] A. S. Sefat, D. J. Singh, R. Jin, M. A. McGuire, B. C. Sales, and D. Mandrus, Renormalized behavior and proximity of  $\text{BaCo}_2\text{As}_2$  to a magnetic quantum critical point, *Phys. Rev. B* **79**, 024512 (2009).
- [45] V. K. Anand, D. G. Quirinale, Y. Lee, B. N. Harmon, Y. Furukawa, V. V. Ogloblich, A. Huq, D. L. Abernathy, P. W. Stephens, R. J. McQueeney, A. Kreyssig, A. I. Goldman, and D. C. Johnston, Crystallography and physical properties of  $\text{BaCo}_2\text{As}_2$ ,  $\text{Ba}_{0.94}\text{K}_{0.06}\text{Co}_2\text{As}_2$ , and  $\text{Ba}_{0.78}\text{K}_{0.22}\text{Co}_2\text{As}_2$ , *Phys. Rev. B* **90**, 064517 (2014).
- [46] W. Jayasekara, Y. B. Lee, A. Pandey, G. S. Tucker, A. Sapkota, J. Lamsal, S. Calder, D. A. Abernathy, B. N. Harmon, A. Kreyssig, D. Vaknin, D. C. Johnston, A. I. Goldman, and R. J. McQueeney, Stripe antiferromagnetic spin fluctuations in  $\text{SrCo}_2\text{As}_2$ , *Phys. Rev. Lett.* **111**, 157001 (2013).
- [47] A. Leithe-Jasper, W. Schnelle, C. Geibel, and H. Rosner, Superconducting state in  $\text{SrFe}_{2-x}\text{Co}_x\text{As}_2$  by internal doping of the iron arsenide layers, *Phys. Rev. Lett.* **101**, 207004 (2008).
- [48] J. Ballinger, L. E. Wenger, Y. K. Vohra, and A. S. Sefat, Magnetic properties of single crystal  $\text{EuCo}_2\text{As}_2$ , *J. Appl. Phys.* **111**, 07E106 (2012).
- [49] R. S. Dhaka, Y. Lee, V. K. Anand, D. C. Johnston, B. N. Harmon, and A. Kaminski, Angle-resolved photoemission spectroscopy study of  $\text{BaCo}_2\text{As}_2$ , *Phys. Rev. B* **87**, 214516 (2013).
- [50] N. Xu, P. Richard, A. van Roekeghem, P. Zhang, H. Miao, W.-L. Zhang, T. Qian, M. Ferrero, A. S. Sefat, S. Biermann, and H. Ding, Electronic band structure of  $\text{BaCo}_2\text{As}_2$ : a fully doped ferropnictide analog with reduced electronic correlations, *Phys. Rev. X* **3**, 011006 (2013).
- [51] J. Mansart, P. L. Fevre, F. Bertran, A. Forget, D. Colson, and V. Brouet, Influence of surface symmetry breaking on the magnetism, collapsing, and three-dimensional dispersion of the Co pnictides  $\text{ACo}_2\text{As}_2$  ( $A = \text{Ba}, \text{Sr}, \text{Ca}$ ), *Phys. Rev. B* **94**, 235147 (2016).
- [52] J. P. Perdew and Y. Wang, Accurate and simple analytic representation of the electron-gas correlation energy, *Phys. Rev. B* **45**, 13244 (1992).
- [53] R. S. Dhaka, R. Jiang, S. Ran, S. L. Bud'ko, P. C. Canfield, B. N. Harmon, M. Tomić, R. Valentí, Y. Lee, and A. Kaminski, Dramatic changes in the electronic structure upon transition to the collapsed tetragonal phase in  $\text{CaFe}_2\text{As}_2$ , *Phys. Rev. B* **89**, 020511(R) (2014).
- [54] V. Brouet, P. -H. Lin, Y. Texier, J. Bobroff, A. Taleb-Ibrahimi, P. Le Fèvre, F. Bertran, M. Casula, P. Werner, S. Biermann, F. Rullier-Albenque, A. Forget, and D. Colson, Large temperature dependence of the number of carriers in Co-doped  $\text{BaFe}_2\text{As}_2$ , *Phys. Rev. Lett.* **110**, 167002 (2013).
- [55] H. Mao and Z. Yin, Electronic structure and spin dynamics of  $\text{ACo}_2\text{As}_2$  ( $A = \text{Ba}, \text{Sr}, \text{Ca}$ ), *Phys. Rev. B* **98**, 115128 (2018).
- [56] D. J. Singh, Properties of  $\text{KCo}_2\text{As}_2$  and alloys with Fe and Ru: density functional calculations, *Phys. Rev. B* **79**, 174520 (2009).
- [57] A. D. Palczewski, R. S. Dhaka, Y. Lee, Y. Singh, D. C. Johnston, B. N. Harmon, and A. Kaminski, Experimental and theoretical electronic structure of  $\text{EuRh}_2\text{As}_2$ , *Phys. Rev. B* **85**, 174509 (2012).
- [58] B. Zhou, M. Xu, Y. Zhang, G. Xu, C. He, L. X. Yang, F. Chen, B. P. Xie, X.-Y. Cui, M. Arita, K. Shimada, H. Namatame, M. Taniguchi, X. Dai, and D. L. Feng, Electronic structure of  $\text{BaNi}_2\text{As}_2$ , *Phys. Rev. B* **83**, 035110 (2011).
- [59] P. Richard, A. van Roekeghem, B. Q. Lv, T. Qian, T. K. Kim, M. Hoesch, J.-P. Hu, A. S. Sefat, S. Biermann, and H. Ding, Is  $\text{BaCr}_2\text{As}_2$  symmetrical to  $\text{BaFe}_2\text{As}_2$  with respect to half  $3d$  shell filling?, *Phys. Rev. B* **95**, 184516 (2017).

- [60] J. Nayak, K. Filsinger, G. H. Fecher, S. Chadov, J. Minár, E. D. L. Rienks, B. Büchner, S. P. Parkin, J. Fink, and C. Felser, Observation of a remarkable reduction of correlation effects in  $\text{BaCr}_2\text{As}_2$  by ARPES, *Proc. Nat. Acad. of Sci. USA* **114**, 12425 (2017).
- [61] Z. P. Yin, K. Haule, and G. Kotliar, Kinetic frustration and the nature of the magnetic and paramagnetic states in iron pnictides and iron chalcogenides, *Nat. Mater.* **10**, 932 (2011).
- [62] P. Starowicz, H. Schwab, J. Goraus, P. Zajdel, F. Forster, J. R. Rak, M. A. Green, I. Vobornik, and F. Reinert, A flat band at the chemical potential of a  $\text{Fe}_{1.03}\text{Te}_{0.94}\text{S}_{0.06}$  superconductor observed by angle-resolved photoemission spectroscopy, *J. Phys.: Condens. Matter* **25**, 195701 (2013).